# The Use of Wave Machinery for Power Generation and Production of Hydrogen as Gas Turbine Fuel

**Pejman Akbari[1]**
*California State Polytechnic University*
*Pomona, CA, 91768, USA*

**Colin D. Copeland[2]**
*Simon Fraser University*
*Vancouver, BC, V3T 4B7, Canada*

**Stefan Tüchler[3]**
*New Wave Hydrogen Inc., Canada*

**Gas turbines present a unique opportunity to generate power outputs and have been widely used in power plants, stationary power generation, and propulsion systems. Increasing concern regarding global warming has urged the gas turbine industry to reduce $CO_2$ emissions from gas turbines. A leading solution is the use of hydrogen as a carbon-free fuel or low-carbon mix in gas turbines. New Wave Hydrogen ($NWH_2$) has developed a revolutionary fuel reformer that thermally decomposes, or cracks, natural gas into hydrogen and carbon black. The innovative method is based on wave rotor technology utilizing shock waves to compress and heat natural gas to temperatures sufficient for methane pyrolysis. This paper introduces the new concept of producing hydrogen using a high-pressure gas source and the $NWH_2$ wave reformer, integrated with a gas turbine, in a flexible range of designs for power generation. Preliminary numerical modeling using an in-house quasi-one-dimensional wave rotor code support the possibility of cracking natural gas in a wave reformer utilizing the energy contained in the combustor burned gas.**

## I. Introduction

The use of hydrogen as a fuel in gas turbines has received considerable attention as an effective way for keeping the combustion process free of gas emissions. Hydrogen is a carbon-free energy carrier with high energy content that is of particular interest in the pursuit of sustainable power generation and the reduction of global $CO_2$ production. It is an abundant element that can be used across a wide spectrum of existing and potential applications including, electrical generation, transportation, propulsion, and heating. Hydrogen can be produced from multiple sources including green hydrogen from water electrolysis using renewable energy [1], gray hydrogen from fossil fuels through natural gas reforming [2], and blue hydrogen combining steam methane reforming (SMR) with carbon capture and storage (CCS). In SMR, methane and steam are heated until they react to yield hydrogen and $CO_2$, further adding to greenhouse gas emissions. To reach the high temperatures necessary to dissociate water (e.g., at around > 2000 K), large thermal energy inputs are required that typically stem from thermal energy generated from hydrocarbon fuels. In addition, the process requires access to water resources for steam production that may be scarce in certain geographical locations.

An alternative is direct thermal decomposition of methane from natural gas (turquoise hydrogen), where methane is decomposed into carbon and hydrogen ($CH_4$ + Heat $\rightarrow$ C + $2H_2$) with trace quantities of other hydrocarbons. This process (methane pyrolysis or methane cracking) is based on the heating of methane to temperatures in which the kinetics of the reaction produce high conversions in a reasonable time. The governing reaction is endothermic, thus the necessary energy input should be provided from an energy source. A main characteristic of this process is the absence of oxygen, which eliminates $CO_2$ and CO by-products. Additionally, no water is consumed, and the produced carbon may have qualities that can be marketed and used in a variety of traditional and novel applications, or it can be securely stored for future use. Different methods of methane pyrolysis have been developed including direct thermal

---

[1] Associate Professor, Electromechanical Engineering Department, AIAA Member.
[2] Associate Professor, School of Sustainable Energy Engineering.
[3] Research Associate, Department of Mechanical Engineering.

cracking at very high temperatures, catalyzed thermal decarbonization, and plasma-torch driven methane pyrolysis [3]. A limited number of these processes have been commercialized. These conversion processes differ in the reactor type, the use of a catalyst, and the source of process-related energy.

New Wave Hydrogen (NWH$_2$) has recently introduced shock-wave compression as the energy source or temperature multiplier for direct thermal methane decomposition [4]. In this approach, a wave rotor [5] is used to generate shock and rarefaction waves for exchanging energy between fluid streams. In combination with the well-known process of methane pyrolysis, one can produce hydrogen at low cost within an efficient reactor. The invention overcomes some disadvantages of the existing techniques by employing shock waves that can produce high temperatures very rapidly with lower energy consumption per unit mass of product. The wave reformer leverages the pressure already in a pipeline or feedstock line, benefiting from the use of the energy embodied in the pipeline flow and energy transfer in the shock wave. The temperature rise required for the fuel decomposition is a function of the pressure differentials between the driver and driven gases, and it is not due to external electricity input. This is an interesting distinction relative to competing methods of methane pyrolysis, i.e., the gas is not heated using electrical or plasma powered sources, it is heated by the rapid compression wave cycle. Thus, the impact of this technology is significant because the production of hydrogen from methane within a wave rotor reformer can utilize existing natural gas supply infrastructure with little change to energy or water supplies.

## II. The Unsteady Pressure Exchanger (Wave Rotor)

Energy exchange/transfer between two fluid flows which are initially at different pressure levels can be accomplished either in indirect fluid-to-fluid interaction or by direct fluid-to-fluid means [6]. As shown in Fig. 1, in indirect energy exchange an intermediate machinery (like a compressor-turbine set) is used, and in direct energy transfer, the fluid-to-fluid process takes place between the two fluids (e.g., air and gas) within an appropriate device with minor mixing between the interacting fluids. Thus, no intermediate mechanical means are required to accomplish the energy transfer in direct fluid-to-fluid machineries. Indirect energy transfer operates based on steady-flow principles and direct transfer devices are often based on unsteady flow. In both approaches illustrated in Fig. 1, the low-pressure air (LPA), used as an example, is energized by the high-pressure gas (HPG) which is being de-energized. In other words, the energy gain (e.g., compression) of LPA to a high-pressure air (HPA) is balanced by energy reduction (e.g., expansion) of HPG to a low-pressure gas (LPG), neglecting the irreversibility and frictional losses. For instance, a shock tube using a high-pressure gas as driver gas and a low-pressure air as driven gas follows the working principles of direct energy-exchange machinery.
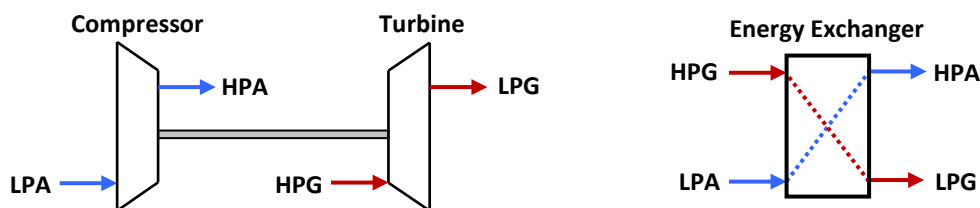


**Figure 1:** Energy exchange between two different fluids using (left) indirect fluid-to-fluid interaction and (right) direct fluid-to-fluid interaction. LPG and HPG refer to low-pressure gas and high-pressure gas, and LPA and HPA refer to low-pressure air and high-pressure air.

### A. Energy Transfer in a Wave Rotor

Wave rotors have been the subject of much past and current research for a century and are described in detail in the literature [5-10]. The wave rotor has been repeatedly recognized as a superior type of energy exchange device [11, 12]. The feasibility of a high-efficiency energy exchange mechanism by using wave rotors has been demonstrated for a variety of applications [13-16]. Wave rotors for gas turbine applications often compress air from a lower to a higher pressure by direct utilization of the energy from a hot, high-pressure combustion gas, thus, they function like superchargers used in automobile engines.

A wave rotor in its simplest form consists of a spinning drum (rotor) with many axial channels arranged unfirmly around its periphery. The drum rotates between two stationary endplates with ports cut in them through which the

channels can communicate with the connecting ducts at pre-determined times. Each channel is periodically charged and discharged as it rotates past properly sized inlet and outlet ports. Phasing differences between edges of the ports enable correct use to be made of pressure and expansion waves generated by the opening and closing of the channel ends, as they pass across the port edges. Figure 2 schematically shows a typical four-port wave rotor. To avoid rubbing, there are finite clearances between the rotor and its endplates. These clearances are exaggerated in the drawing for clarity, but in practice the endplates are placed as closely as possible to the rotor to reduce unavoidable leakage from the channels. The rotor is often driven by a shaft supported by bearings positions on the endplates. The shaft can be powered directly by an external motor or by a crankshaft through a belt transmission. Alternatively, the rotor can be self-driving either by curving the rotor [17] channels or by properly directing the inlet gas at an angle to a straight-bladed rotor [18].
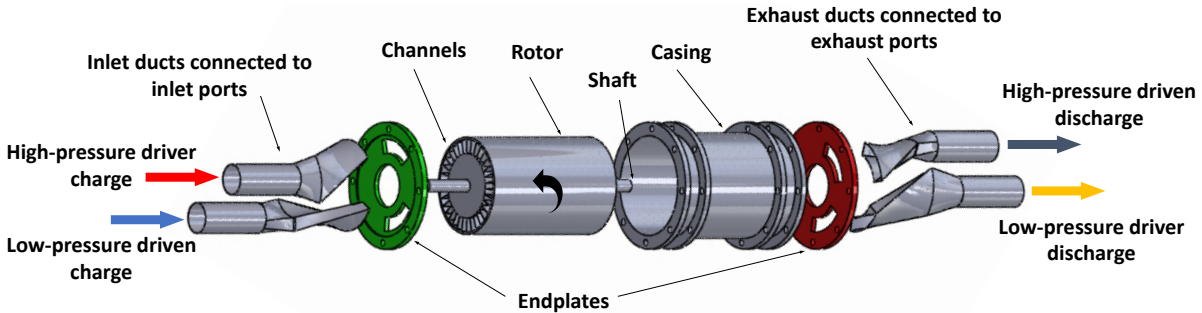


**Figure 2:** Schematic configuration of a four-port wave rotor.

In Fig. 2, the low-pressure driven gas is directed into the wave rotor at its corresponding intake port. The gas flows into the channels on the rotor and remains in the channels until it is exposed to the driver gas when its intake port opens. The high-pressure driver gas which continuously enters the wave rotor channels provides the necessary pressure differential to drive a shock into the driven gas trapped onboard as the channels come into contact with the driver gas intake port. The energized driven gas leaves the rotor from an outlet port at a higher pressure than when it enters the wave rotor. Through drum rotation, the de-energized driver gas leaves the wave rotor through its corresponding outlet port to any suitable apparatus capable of utilizing the heat remained in the exhaust gases. Thus, the wave rotor offers the functions performed by a compressor for the driven gas and functions performed by a turbine for the driver gas in one device without using conventional blades or vanes. Because the compression and expansion are accomplished solely by unsteady waves within the channels, no moving parts are required, with the exception of the rotor. With many channels passing the ports at a high frequency, the flow in the inlet and outlet ports is nearly steady (with some pulsation) and the flow unsteadiness is mostly confined onboard the rotor. Thus, wave rotors can be integrated with conventional steady-flow machineries like compressors and turbines.

### III.   Previous Wave Rotor Applications for Gas Turbines

The first practical wave rotor configurations were reported in the 1940's by Seippel [19, 20]. He envisioned wave rotors as a gas generator driving a turbine and as a high-pressure stage for a gas turbine for a locomotive. Figure 3 illustrates the concept of using a wave rotor as a gas generator. In this system, the wave rotor draws LPA from the surroundings through an LPA intake port. The air in the channel is compressed when it comes into contact with the HPG intake port that receives a portion of the HPG leaving the steady-flow combustion chamber. The air is compressed to nearly the same pressure level as that of the hot gases, or even higher by a multi-shock process in the channel, and is then routed
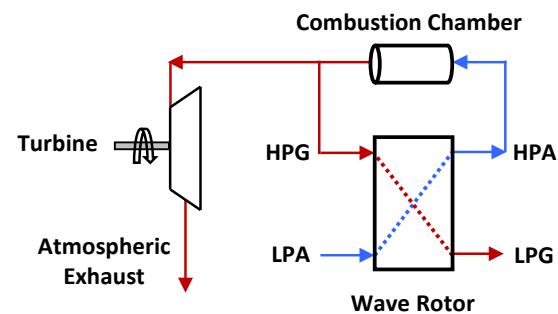


**Figure 3:** Wave rotor acting as a gas generator unit. LPG, HPG, LPA, HPA refers to low-pressure gas, high-pressure gas, low-pressure fresh air, and high-pressure fresh air, respectively.

3

to the combustion chamber. Thus, the wave rotor functions similar to a compressor, increasing the pressure and temperature of the LPA before heat is added in the combustion chamber. The HPA is mixed and burned with fuel in the combustion chamber which connects the HPA and HPG ports. The remaining portion of HPG is delivered to a turbine for power extraction. It expands in the turbine and is exhausted into the surroundings. Meanwhile, that portion of the HPG that expands across the wave rotor by expansion waves within the rotor channels is sent to the atmosphere as LPG. As an analogy, the wave rotor operates like a turbine between HPG and LPG ports. Therefore, the wave rotor provides the equivalent of a coupled compressor and turbine but does so with less complicated machinery, at less cost, and with less space requirement [21].

A design scheme for such a gas generator unit is shown in Fig. 4 where a heat exchange is added to the system to preheat the compressed air leaving the wave rotor using the remaining heat in the turbine exhaust gas [22]. In this layout, commonly known as the reverse-flow wave rotor configuration, the fresh air enters and exits on one side of the rotor and the burned gas enters and exits on the other end of the rotor. The reverse-flow arrangement was extensively tested by BBC (Brown Boveri), and their commercialized wave rotor used as a supercharger for diesel engines (a.k.a Comprex) was designed based on this port arrangement [23]. It is also possible to use the wave rotor for shaft power extraction (a.k.a. wave engine) with angled blades, eliminating the external turbine, as demonstrated by Pearson [24] and others [25-27] in the past, and recently revisited by Copeland and Tüchler [17, 28]. Welch [29, 30] and Nalim [31] have also studied gas generator units using two-port wave turbines with on-rotor combustion that further eliminates the external combustion chamber.
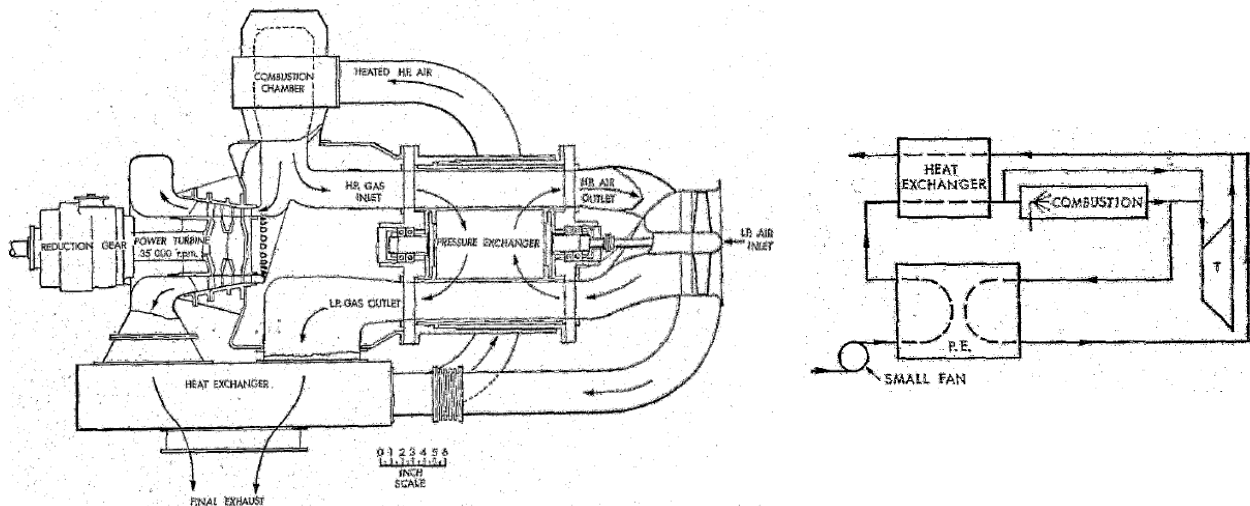


**Figure 4:** Design arrangement for a gas generator using a four-port pressure exchanger (P.E.) and a heat exchanger, taken from Ref. [22].

Seippel also proposed a wave rotor as a second stage for a gas turbine unit by connecting the LPA port to a compressor delivery and the LPG port to a turbine inlet. Consequently, two possible arrangements were studied and reported in the literature. In the first arrangement [21, 32-34], shown in Fig. 5 (left), the compressed air from the compressor outlet enters the wave rotor (2) where it undergoes a further compression process by shock waves. The double-compressed air (3) is heated up in a combustion chamber. The combustion gases are split into two streams. The first stream is directed to a high-pressure turbine (5) which would provide shaft power for various applications. The reaming stream is further heated in the combustion chamber. This increase in temperature poses no threat to the turbine blades because the wave rotor is placed directly downstream of the combustion chamber, and the hot gas from the combustor is cooled within the wave rotor before flowing into the second turbine. The hot gas (driver gas) is directed to the wave rotor (4) to compress the compressor delivery air (driven gas).
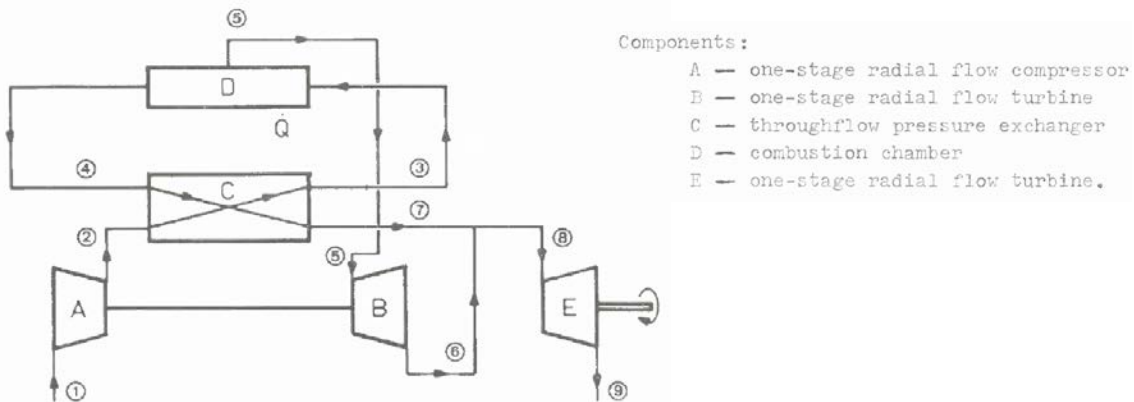
Figure 5 (right) schematically shows an enthalpy-entropy diagram of the cycle. Due to the addition of a compressor to the unit, the cycle's overall pressure ratio and peak temperature are increased compared to a baseline engine without a wave rotor. Burned gas entering the free-power turbine could be optionally cooled (not shown in the figure) with the cooler high-pressure air exiting the wave rotor (3) to meet the allowable turbine inlet temperature [6]. The expanded hot gas leaving the wave rotor (7) is mixed with the free-power turbine exhaust gas (6) and later enters a secondary turbine (8) which drives the compressor, i.e., the baseline turbine. The baseline turbine operates at the same

4

temperature and pressure as a conventional gas turbine, thus, the total gain in power output of the wave rotor topping cycle corresponds to the power output of the high-pressure turbine, as the wave rotor with straight channels produces zero shaft power. Because wave rotors allow higher cycle pressure ratios and higher peak temperatures, the wave rotor topping cycle is more efficient than an untopped (baseline) engine. As described later in this study, current versions of wave rotor topping cycles do not usually bleed hot gases from the combustion chamber to the high-pressure turbine, and a simpler system arrangement with only one turbine is often used.
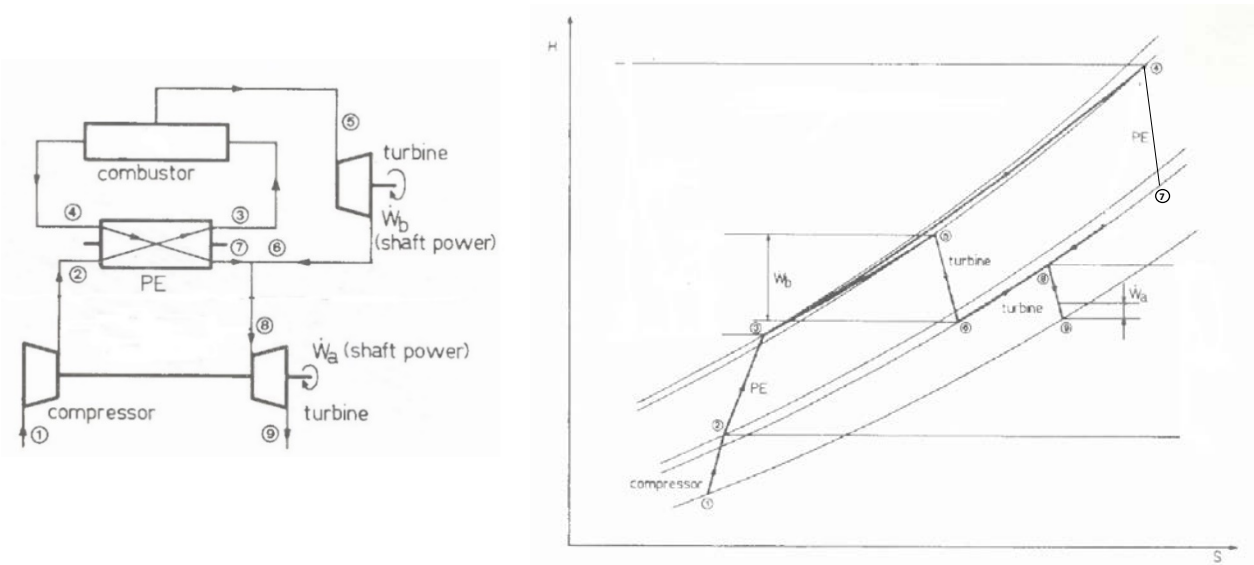


**Figure 5:** Left: schematic of topping a gas turbine with a four-port pressure exchanger (PE), Right: corresponding enthalpy-entropy diagram, adapted and modified from Ref. [32].

In an alternative arrangement [32, 35], as schematically shown in Fig. 6, the bypass gas from the combustion chamber enters the baseline turbine (5) first and later the turbine exhaust gas (6) is combined with the outlet gas from the low-pressure gas outlet port of the wave rotor (7) before entering the free-power turbine inlet (8). This arrangement was later adapted by Mathematical Science Northwest (MSNW) to be used in a turbofan engine [36]. MSNW was studying wave rotors to improve the performance of small turbofan engines [37]. Fig. 7 shows an integration of a four-port wave rotor to a turbofan engine, which is similar to the cycle displayed in Fig. 6 proposed for a ground-based gas turbine engine.



Components:
A — one-stage radial flow compressor
B — one-stage radial flow turbine
C — throughflow pressure exchanger
D — combustion chamber
E — one-stage radial flow turbine.

**Figure 6:** Schematic of topping a gas turbine with a four-port pressure exchanger (PE), adapted from Ref. [32].
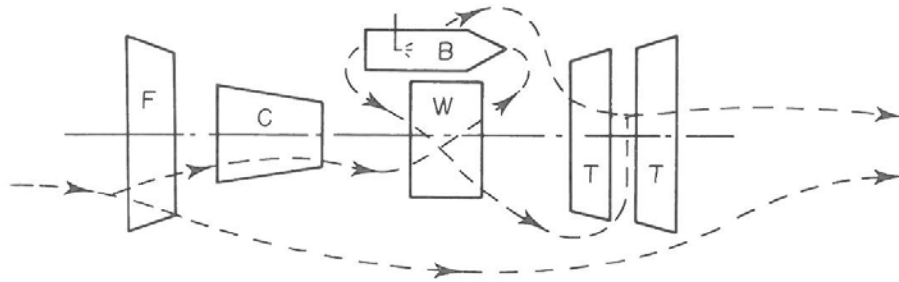
**Figure 7:** Schematic of a turbofan engine topped by a four-port wave rotor (W), adapted from Ref. [36].

Keller from Asea Brown Boveri (ABB) in Switzerland proposed [33] a wave rotor enhanced gas turbine cycle with two combustion chambers and an afterburner, as shown in Fig. 8, which was later examined at ABB [34]. In this arrangement, the supercharged air leaving the wave rotor (8) is divided between the two combustion chambers. The driver gas for the wave rotor (8b) is first heated in the first combustion chamber (indicated by arrow 16) and heated again in the afterburner (indicated by arrow 19) before entering the wave rotor. The rest of the air (8a) is heated in the second combustion chamber (indicated by arrow 11) and at a high pressure enters (12) the free-power turbine (13), driving a generator (14). The partially expanded gas leaves the turbine (15) and mixes with the pre-expanded driver gas flowing out of the wave rotor (20). This hot gas mixture (21) is passed into the baseline turbine (3) which drives the compressor (1).
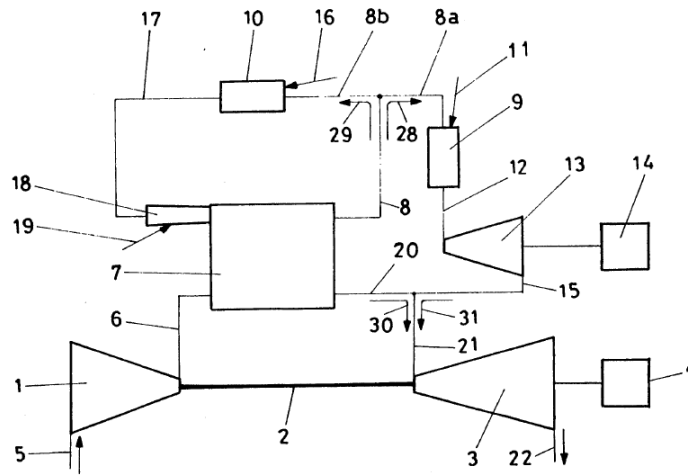


**Figure 8:** Schematic of topping a gas turbine with a four-port wave rotor proposed by Keller at ABB, adapted from Ref. [33].

Weber has also described [12, 26] a wave rotor topping cycle that uses two turbines and a five-port wave rotor, as schematically shown in Fig. 9. In this arrangement, the wave rotor has three outlet ports, two of which are connected to a high-pressure (HP) and a low-pressure (LP) turbine. The burned gas entering the wave rotor (5) is divided between two outlet ports through two expansion stages. The gas expanded in the first stage is directed to the HP turbine (12) for power production. The remaining gas, which expands in the second stage, enters the LP turbine (15), which drives the compressor. The HP and LP turbine outputs exhaust into the atmosphere after utilizing hot gases to drive them.

6
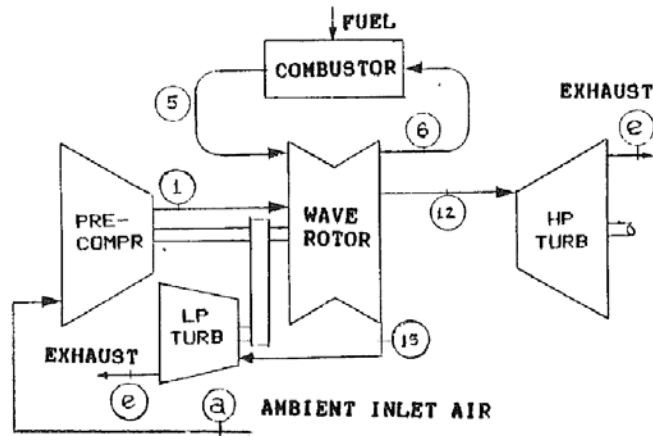
**Figure 9:** Schematic of topping a gas turbine with a five-port wave rotor, adapted from Refs. [12, 26].

In all the above examples, compressed air was used as the driven gas. There have been other gas turbine cycles in which energy exchange is obtained between a hot driver gas and a cooler turbine working gas used as the driven gas. These cycles were first introduced and studied by researchers at Cornell Aeronautical Laboratory (CAL) in the early 1950s [13] and later explored by others [38-40]. Figure 10 illustrates the application of the wave rotor to a simple steam power cycle [13]. The wave rotor was placed between the combustion chamber and the turbine. The hot, high-pressure gas leaving the combustion chamber was the driver gas for the wave rotor. In operation, it would expand and leave the rotor on the same end from which it entered. Steam used as the driven gas would enter and leave from the opposite end. The energized steam in this loop would drive the power turbine to extract power. Thus, the available energy from the hot combustion gas expansion would transfer directly to the steam, providing a high-pressure flow of steam to the turbine. There are several operational advantages in this arrangement. For instance, a higher peak temperature from the hot combustion products, even above the capabilities of turbine cooling technologies, could be utilized to power the turbine because the turbine blades were not exposed to the hot combustion gases. Also, two different fluid streams could be used in this cycle where the burned gas in the driver-fluid loop was separated from the steam through the turbine. More complicated steam power cycles utilizing intercoolers, reheaters, and heat exchangers were also proposed and studied by Hertzberg and Weatherston [13]. Their work later formed a number of advanced power generation cycles studies by MSNW [38-40] who investigated wave rotor application for pressurized fluidized coal-burning combined cycle power plants.
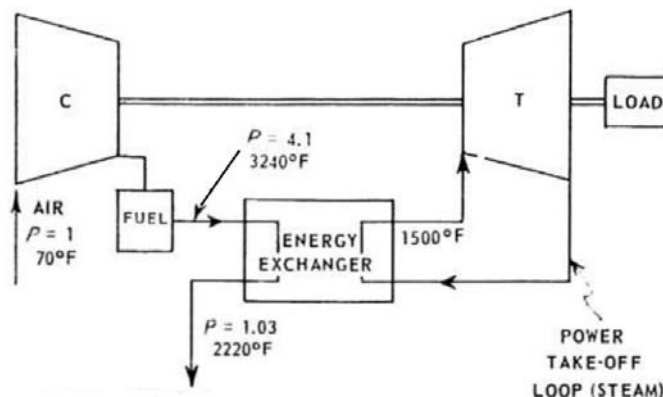


**Figure 10:** Steam power cycle topped by a four-port wave rotor, adapted from Ref. [13].

Hertzberg et al. at CAL also pursued the idea of air shock heating to produce NO and combining it with water to produce nitric acid ($HNO_3$) as a final product [41]. Their studies led to a successful series of experiments which

7

demonstrated that nitrogen could be fixed by means of unsteady compression and expansion waves within wave rotor channels as a method of commercial nitrogen fixation. A schematic layout of a cycle producing $HNO_3$ is shown in Fig. 11.
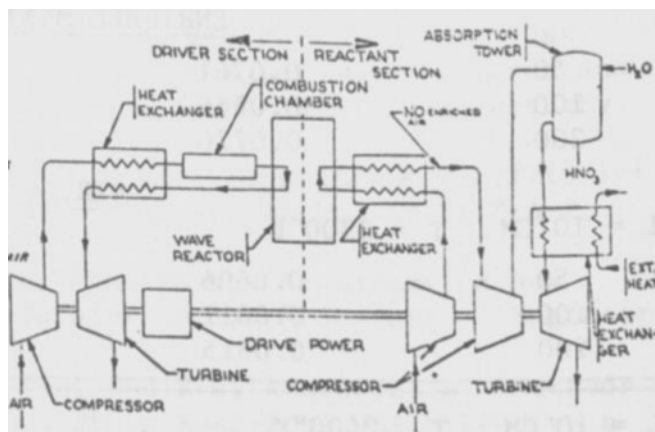


**Figure 11:** Schematic of a cycle designed to produce nitric acid, adapted from Ref. [41].

The cycle consists of two major parts: (i) driver section, and (ii) reaction section. The driver section (left) is designed to provide hot high-pressure driver gas to carry out the compression process in the wave reactor. In this section, air enters a compressor driven by a turbine which is partially driven by a motor. The compressed air is directed to a heat exchanger where it picks up heat and then is directed to a combustion chamber. In the combustion chamber the preheated compressed air and fuel mixture is combusted to provide a hot, high-pressure combustion driver gas for the wave reactor. After the driver gas has expanded within the wave reactor, the low-pressure exhausted driver gas is discharged into the heat exchanger in which some of the heat of the discharged driver gas is given up to the compressed air leaving the compressor. After leaving the heat exchanger, the cooled driver gas is directed to the turbine wherein the energy of the driver gas is utilized to drive the turbine. Finally, the driver gas is discharged from the turbine to the atmosphere. On the reactant gas side, the reactant gas (air) is preheated through a heat exchanger after being raised to an appropriate pressure by a compressor. The preheated reactant gas then enters the wave reactor opposite from the end at which the driver gas inlet and outlet ports are located. After the reactant gas is processed within the reactor, the heated processed gas enriched with NO is discharged to the heat exchanger where it transfers some of its heat to the reactant gas entering the reactor. The cooled processed gas leaving the heat exchanger is directed to a secondary compressor to raise the gas pressure before entering an absorption tower. Water is injected and mixed with NO in the tower, producing $HNO_3$, which is then collected from the bottom of the tower. The remaining gas is directed to a secondary heat exchanger and a turbine which drives the two compressors used in the reaction gas section of the cycle.

Another idea for topping a gas turbine by with wave rotor was proposed by Hertzberg and Christiansen at the University of Washington in the mid 1990s [42]. Figure 12 shows a gas turbine cycle topped by a four-port wave rotor. In this arrangement, a compressed mixture of fuel (1) burns within the rotor channels (2), i.e., an onboard-combustion wave rotor. By accomplishing combustion on the rotor, the external combustor is no longer needed. The combustion process occurs when both ends of the channels are closed (e.g., constant volume combustion), leading to an additional pressure rise of the gas. Meanwhile, the driver gas entering and leaving from the opposite end is also sufficiently compressed by the combustion process so that additional work can be extracted by a topping turbine. The combustion product gas leaving the rotor (3) is still at a high enough pressure that its energy can be extracted by the bottoming turbine (4-5). Hence, the driver gas is energized by compression energy inside the rotor,
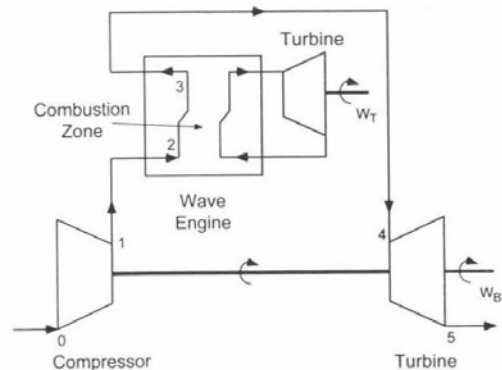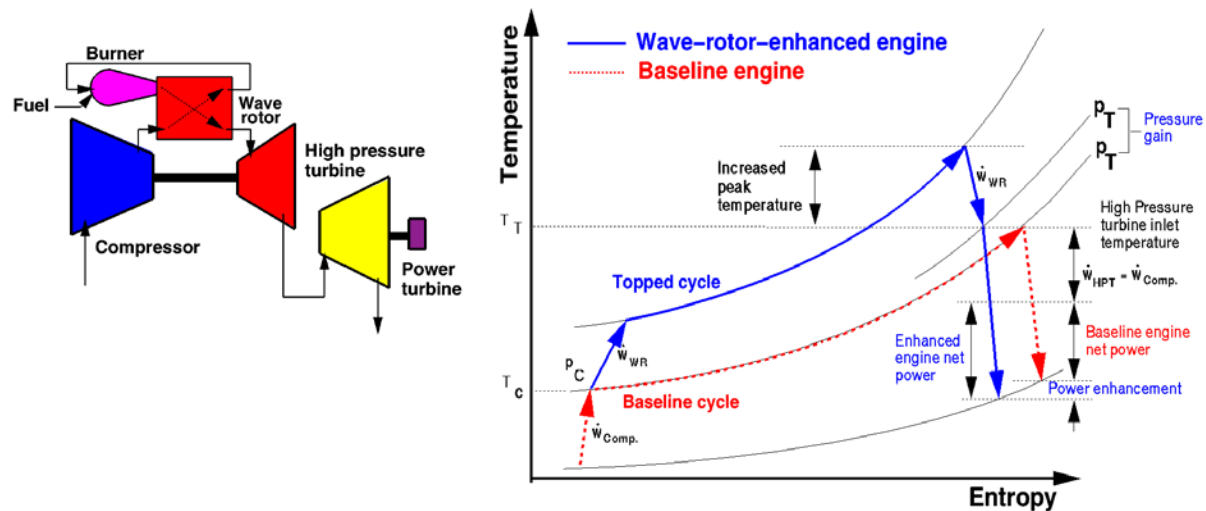


**Figure 12:** Topping a gas turbine with a four-port onboard combustion wave rotor, adapted from Ref. [42].

8

creating a "fly-wheel" type of driver system. This allows a stand-alone turbine to be used in the driver gas circulation loop without auxiliary equipment. No prototype of this novel concept has been reported.

Circa 1989, NASA Glen Research Center (GRC) initiated a wave rotor program focused on gas turbine topping cycles [43], in part building on wave rotor development programs at ABB [34] and at other research institutes [14, 44, 45]. In a close collaborative work by the U.S. Army Research Laboratory and Rolls-Royce Allison, extensive numerical and experimental efforts were conducted with wave rotors to enhance the performance of turboshaft engines [46-49]. An excellent overview of the NASA GRC investigations during 90's has been reported by Welch [10]. Figure 13 (left) is an example of a few cases that were extensively studied by NASA with the corresponding temperature-entropy diagram shown on the right [50]. The hot combustion gas enters the wave rotor where it expands and flows into the high-pressure turbine that drives the compressor. The hot gas that partially expands in the first turbine then drives the second turbine which provides power output. This arrangement is less complex than those described in Figs. 5, 6, and 8 because the entire gas product leaving the combustion chamber is directed to the wave rotor. Figure 13 (right) indicates that in the wave-rotor-topped engine the high-pressure turbine entry pressure is greater than the pressure of the air delivered by the compressor for the same turbine inlet temperature used in the baseline engine. Hence, by using a wave rotor, a pressure gain additional to that provided by the compressor is obtained. Thus, more power can be extracted in the enhanced engine compared with the baseline engine with equivalent heat addition, resulting in an increased engine efficiency and reduced specific fuel consumption.



**Figure 13:** Left: topping a gas turbine with a four-port combustion wave rotor (WR), Right: corresponding entropy-temperature diagram, adapted from Ref. [50].

To illustrate the application of a wave rotor for a gas turbine engine with a numerical example, Fig. 14 is presented which shows a known design point operating schematic of a small turboshaft engine topped by a wave rotor. This study was conducted by Snyder and Fish [51] using the Allison 250 Series Engine as the baseline engine. To allow operating temperatures of turbine blade materials to be within reasonable values, the turbine inlet temperature is held to a baseline engine level (1330 K). However, the burner exit temperature is at a higher level of 1703 K. Meanwhile, the pressure in the burner is increased by the compression ratio of the wave rotor; hence, the burner inlet operates at a pressure ratio of 3.37 higher than the compressor discharge. Thus, the burner of the enhanced engine experiences higher pressures and temperatures than the baseline engine. Gas expansion within the wave rotor experiences a 373 K reduction in gas temperature when the burned gas arrives to the turbine inlet section. Despite a pressure loss of approximately 9% across the burner, a 24% pressure gain is obtained between the compressor discharge and the turbine inlet. Consequently, results of the study indicated a significant performance improvement for the enhanced cycle. The baseline engine produces a nominal 485 kW (650 hp) power at maximum continuous rating with a specific fuel consumption (SFC) of 0.100 (0.59 lbm/hr/hp). It was determined through mathematical modeling that the demonstrator engine has a predicted 547 kW (733 hp) power with an SFC of 0.076 (0.45 lbm/hr/hp). Thus, application of the wave rotor is predicted to yield a 13% increase in power with a 23% decrease in SFC.
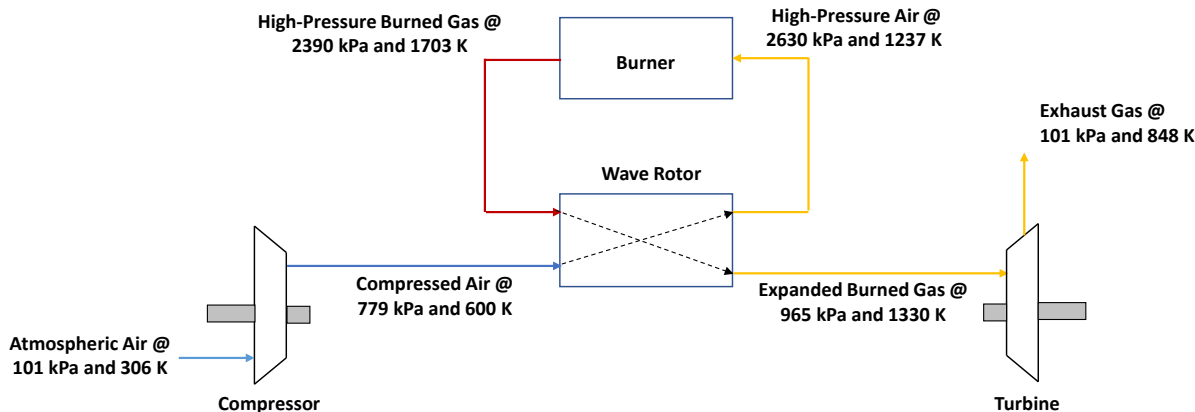
**Figure 14:** Engine design point cycle conditions for the Allison 250 Series Engine topped by a wave rotor, adapted from Ref. [51].

## IV.  Methane Pyrolysis Using the Wave Reformer

Recently, NWH$_2$ has proposed hydrogen production through compression-induced pyrolysis of methane using the pressure in natural gas pipelines [4]. Figure 15 illustrates one example of several NWH$_2$ designs for natural gas reforming. Here, the high-pressure natural gas (95-100% methane) supply is preheated in a heat exchanger (not shown) where it picks up heat from the high-temperature carbon-lean fuel and enters the wave reformer high-pressure inlet port at State 2. This hot, high-pressure gas mixture initiates the shock heating process onboard the wave reformer and compresses the driven gas which is already in the channels. The driver gas is expanded within the channels and exits the wave reformer through a low-pressure outlet port at State 3. Upon exiting the rotor, the outlet gas is slightly compressed by a low-pressure compressor (State 5) to overcome pipe pressure losses, providing the fuel that will be reformed onboard the wave reformer. Additionally, a heater is placed in this loop to add heat to the fuel. This heater sets the temperature of the fuel to be reformed to the appropriate value as it enters the wave reformer low-pressure inlet port at State 6. Thus, the fuel is converted from a driver gas to a driven gas with the aid of the low-pressure recirculation loop. This distinguishes the wave reformer from typical pressure-exchange wave rotors where two distinct working fluids are typically used as driver and driven gases. The heated driven gas reformed by the expansion of the driver gas onboard the rotor is routed out of the reformer high-pressure outlet port at State 7. This stream is the hot, moderate-pressure product stream composed of hydrogen, carbon, and a fraction of unreformed methane with possible minor byproduct constituents. The gas can be routed to a gas cyclone and/or baghouse or a similar system to separate the gas and solid products. In this arrangement, the wave reformer is integrated into the system such that all the natural gas at a high pressure is routed through the system where approximately 20% of the fuel is reformed into a carbon-lean fuel stream and the remaining fuel (~80%) is routed back to the reformer at a reduced pressure.

Figure 16 describes the wave diagram for the four-port wave reformer introduced in Fig. 15. This figure schematically illustrates an unwrapped demonstration of the wave reformer with only one channel shown moving upward. The wave diagram in general portrays the annular arrangement of the inlet and outlet ports, the solid walls reflecting the endplates, the wave fronts, and
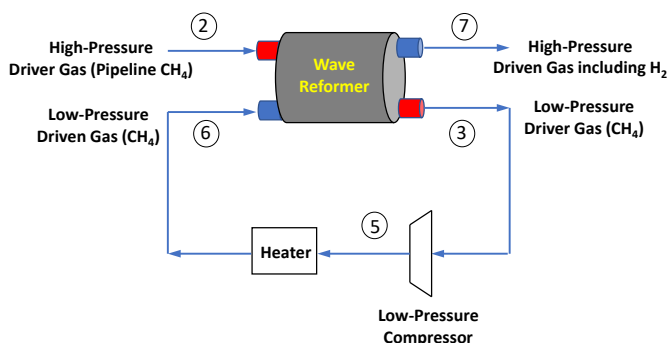


**Figure 15:** Thermal decomposition of methane using a wave reformer.

the gas interfaces during each phase of the cycle. In the wave diagram, the horizontal axis represents the rotor axial length and the vertical axis is time (or rotational angle). The top of each wave diagram is looped around and joined to the bottom of the diagram, because each wave cycle is repetitive. The vertical black rectangles on each side of the channels represent the stationary endplate locations around the circumference when the inlet and outlet ports are closed. The diagonal lines are the propagation lines (trajectories) of the waves or contact surfaces (interfaces between the fluids). The port numbers (2, 3, 6, 7) correspond to those used in Fig. 15. The red or darker gray area represents the driver gas (pipeline natural gas) and blue or lighter gray area represents the driven gas (methane to be reformed). The cycle consists of the following steps: charging of reactant gas into the reformer, charging of driving gas into the reformer, removal of reactant products from



**Figure 16:** Wave diagram of a four-port wave reformer.

the reactor, and removal of spent driver gas from the reactor. The last two processes often occur simultaneously.

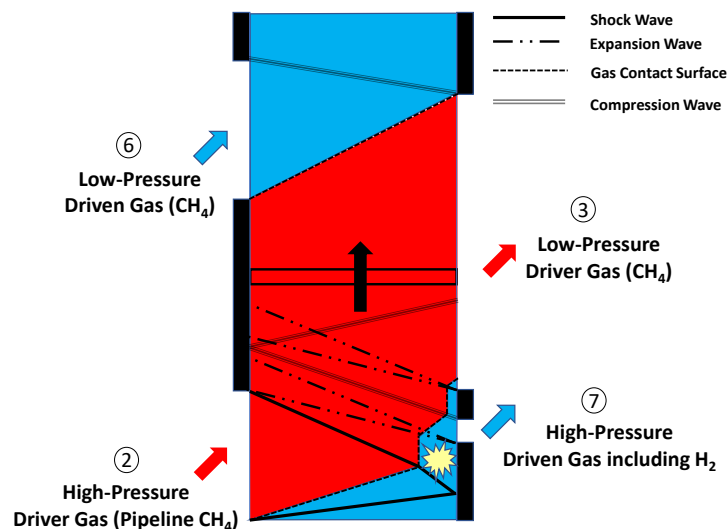The cycle starts from the bottom of the diagram where the primary shock wave compressing the reactant gas (e.g., pipeline natural gas) is deliberately timed to strike the solid endplate at the far-right end of the channel so that it can reflect from the endplate, stagnating the channel flow. It is well recognized that the temperature behind a reflected shock wave is approximately double that behind an incident shock wave, therefore, higher temperatures can be attained by shock reflection. Hence, the reflected shock wave passes through the reactant gas whose temperature has been raised to an intermediate level by the first shock wave, thereby raising the temperature of the process gas to an even higher level, i.e., maximum temperature. This peak temperature is sufficient to permit methane thermal decomposition prior to opening the exit port. The peak temperature in the reaction zone (highlighted by the yellow mark) is a function of the initial temperature of the reactant gas and the Mach number of the primary shock wave, which is specified by the pressure ratio between the driver gas and the reactant gas. The passage of the reflected shock wave brings the reactant gas and the driver gas to rest as indicated by a vertical-line contact surface separating two gases. Sufficient reaction time (the time during which the reactant gas is heated by the shock wave) may be provided by adjusting the rotor speed, the channel length, and flow conditions. The reaction continues until the opening of the driven gas exit port. When the right end of the channel opens (i.e., exposed to the exit port), an expansion wave (dashed-dotted line) is generated from the lower corner of the exit port propagating to the left, reducing the processed gas (e.g., products) temperature. The reaction time onboard the rotor is terminated after the processed gas is expelled from the end of the channel by the action of the cooling expansion wave. Thus, the duration of the maximum temperature attained by the processed gas is limited by opening the exit port. This time is usually in the order of milliseconds for practical rotor speeds. With steady rotation of the channels and a cyclic sequence of events occurring in the reformer, production of hydrogen for relatively long periods can be attained (even without cooling), greatly exceeding the useful duration of up to only few milliseconds [52] obtained by a typical chemical shock tube that has only a single channel and a limited production capacity.

A combination of a hammer shock generated by closing the product exhaust port and another expansion fan generated by opening the driver gas outlet port aids the scavenging of the driver gas from the downstream end of the rotor. After further rotation of the channels, fresh preheated reactant gas enters the channel from the left by opening the driven gas entry port. This gas separated by a contact surface from the driver gas leaving the channel from right creates an overlap process. While the overlap process continues, the scavenging of the driver gas through the exit port is terminated by closing the exhaust port. The closing of the exhaust port is timed with the arrival of the driven gas to the right end of the channel. Closing the exhaust port generates another compression wave propagating to the left stopping the flow of the reactant. When the compression wave meets the upper corner of the inlet port, the port closes, leaving the channel fully filled with fresh reactant gas and the next cycle can be initiated.

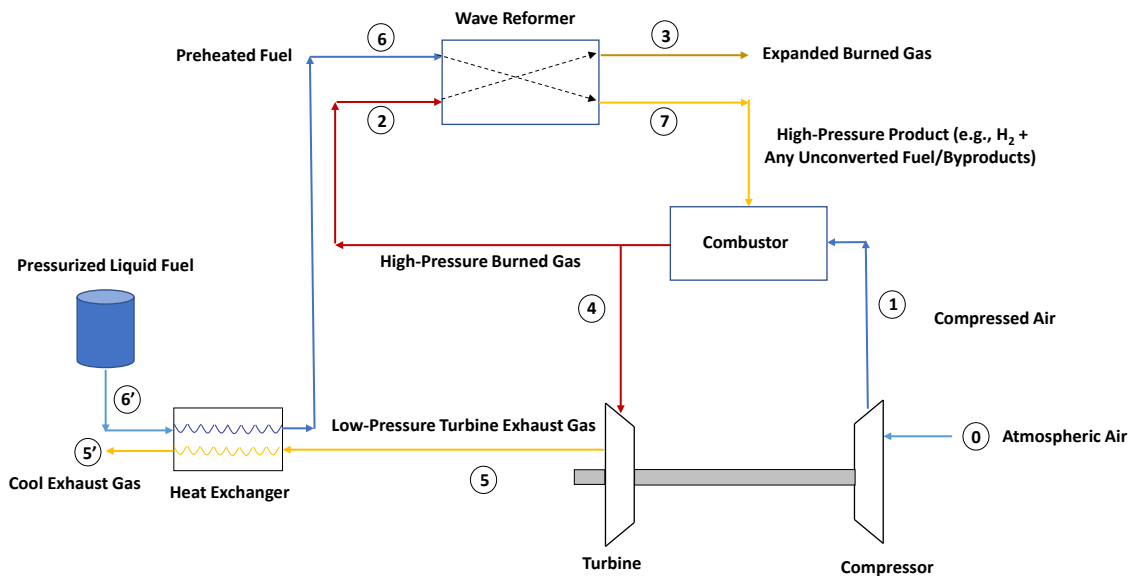# V.  Wave Reformer Integrated with a Gas Turbine

In the following, three system configurations will be discussed for integrating a wave reformer to a gas turbine cycle. These three potential applications are referred to as:

(A) Wave reformer integrated in a gas turbine and producing hydrogen fuel to drive the gas turbine cycle.

(B) Producing fuel in-line for delivery to a gas turbine cycle.

(C) Dual rotors integrated in a gas turbine cycle, producing fuel and pressure gain between compressor and turbine.

In all three cases introduced above, the initial input or fuel source for the power generation system can be any gaseous hydrocarbon fuel (i.e., $C_xH_y$).

## A.  Wave reformer integrated in a gas turbine and producing hydrogen fuel to drive the gas turbine cycle:

The schematic shown in Fig. 17 illustrates how the new gas turbine engine cycle works. The engine uses compressed air (State 1) entering the combustor. Meanwhile, hydrocarbon fuel from a fuel tank, pre-heated by a heat exchanger is directed into the wave reformer (State 6) through the first port of the reformer. When the first port is opened, the gaseous fuel flows into the channels of the rotor and is further compressed by at least one shock wave. Such a shock compression can amplify the temperature of the fluid high enough for thermal decomposition, with hydrogen as a product. As the rotor is rotating, when the channel aligns with the second port in the endplate, the channel is then opened, and the produced hydrogen leaves the rotor (State 7). This produced hydrogen is injected into the combustor. After the combustion process within the combustor, the high-pressure burned gas splits into two segments. A small portion of it is delivered to the reformer (State 2) through the opening of a third port. It is acknowledged that bleeding gas from the combustor to the wave reformer would reduce the power produced in the turbine, thus, the amount of hot gas bled from the combustor should be as low as possible. The incoming high-pressure burned gas from the combustor (driver gas) triggers a shock wave in the rotor channel, compressing the fuel (driven gas) residing in the channels. After the wave rotor spins around to a fourth port in the reformer, the burned gas trapped within the channels expands and flows to the surroundings (State 3). It might be preferred to use this gas to preheat the high-pressure fluid at State 1 before it enters the combustor using a secondary heat exchanger (not shown). The remaining (majority) of the burned gas is delivered to the turbine (State 4). After work extraction in the turbine, the gas exits the turbine (State 5) and enters the heat exchange that heats up the liquid ammonia entering the heat exchanger from a fuel tank at State 6′. The liquid fuel vaporizes across the heat exchanger and is directed to the wave reformer at State 6. Therefore, in this novel system arrangement, the reformer provides clean hydrogen fuel for the combustor using the energy contained in the burned gas. This arrangement is a new application of wave rotors in ground-based gas turbines, where the production of hydrogen as clean fuel is an integrated part of the turbine system.



**Figure 17:** Wave reformer integrated in a gas turbine and producing hydrogen fuel to drive the gas turbine cycle.

The numerical tool used to predict the wave reformer port conditions is a quasi-one-dimensional wave rotor code developed and experimentally validated by Tüchler and Copeland in conjunction with their wave rotor studies at University of Bath, UK [17, 28, 53]. The model discretizes and solves the laminar one-dimensional Navier-Stokes equations using a two-step Richtmyer TVD scheme with minmod flux limiter in a time-marching manner. The code follows a single, constant-area wave rotor passage as it rotates along the circumference and is exposed to boundary conditions imposed by the respective port arrangement.

The governing equations are as follows:

$$\frac{\partial \vec{U}}{\partial t} + \frac{\partial \vec{F}}{\partial x} = \vec{S}$$

(1)

The state vector $\vec{U}$, flux vector $\vec{F}$ and source term vector $\vec{S}$ are:

$$\vec{U} = \begin{pmatrix} \rho \\ \rho u \\ \rho E \\ \rho Y_i \\ \vdots \\ \rho \dot{Y}_n \end{pmatrix}, \qquad \vec{F} = \begin{pmatrix} \rho \\ \rho u \\ \rho E \\ \rho Y_i \\ \vdots \\ \rho \dot{Y}_n \end{pmatrix}, \qquad \vec{S} = \begin{pmatrix} 0 \\ 0 \\ \dot{\omega}_T \\ \dot{\omega}_i \\ \vdots \\ \dot{\omega}_n \end{pmatrix}$$

(2)

Where $\rho$ denotes the density of the mixture, $u$ the velocity in x-direction, $p$ the static pressure and $E$ the total energy per unit volume. The model incorporates transport equations for species and corresponding source terms to account for the pyrolysis of reactants into products using a global, one-step reaction equation. The quantity $Y_i$ represents the mass fraction of each chemical specie satisfying the following equation:

$$\sum_{i=1}^{n} Y_i = 1, \sum_{i=1}^{n} \dot{\omega}_i = 0$$

(3)

where $\dot{\omega}_i$ represents species mass reaction rate. In addition, it is assumed that each specie follows the ideal gas law:

$$p = \rho R T \sum_{i=1}^{n} \frac{Y_i}{W_i}$$

(4)

with $R$ used as the universal gas constant.

The source terms accounting for the chemical reaction contain $\dot{\omega}_i$ and the endothermic heat absorption $\dot{\omega}_T$. The production rate and the heat absorption follow:

$$\dot{\omega} = \nu k_f \rho Y$$

(5)

$$\dot{\omega}_T = -Q\dot{\omega}$$

(6)

where $\nu$ represents the stoichiometric coefficient and $Q$ the heat absorption per unit mass of reactant.

The reaction rate $k_f$ is described by the simple Arrhenius law of $k_f = A\, exp\left(-\frac{E_a}{R_m T}\right)$, where $A$ denotes the pre-exponential factor, $E_a$ the activation energy and $R_m$ the molar gas constant.

The reactive model in this study to examine the conversion of methane within a wave reformer follows the simplified reaction equation:

$$CH_4 \rightarrow \text{Products}$$

13
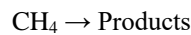
Here, it is assumed that the products are primarily consisting of hydrogen, ignoring solid carbon black and intermediate products.

Methane pyrolysis been studied extensively in the literature [54-63], suggesting a wide range of Arrhenius parameters. For example, in Fig. 18, where the rate constant is plotted against temperature, pre-exponential factors can vary between ~8.5E+9 and ~5.1E+14 and activation energies between 312,000 and 431,200 depending on the type of reactor, the considered temperature range and residence time and the initial molar fraction of methane.
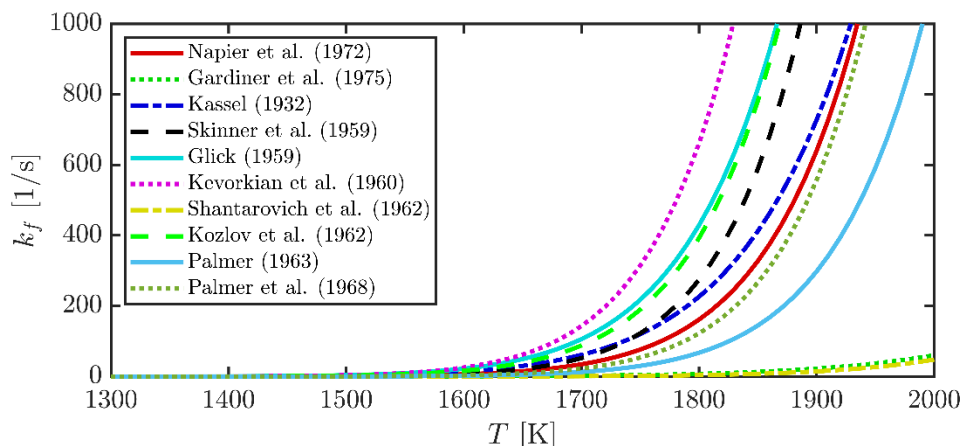


**Figure 18:** Temperature-dependent rate constant for global, one-step reaction $CH_4 \rightarrow$ Products

To examine the sensitivity of the numerical model to the choice of Arrhenius coefficients, a shock tube study was set up with a driver and driven arrangement. The driver section is filled with $N_2$ at 40 atm and 2000 K, while the driven section is filled with pure $CH_4$ at conditions of 1 atm and 400 K. Both sections are set to zero velocity at t=0. Figure 19 shows the solutions in form of *x-t* plots that exhibit pressure, temperature, Mach number and gas velocity in the tube. The corresponding species contours are shown in Fig. 20 which illustrate distributions of the reactant ($CH_4$), the product ($H_2$) and the driver gas ($N_2$) using the kinetic parameters by Kevorkian et al. where $A = 1.3E+14$ and $E_a$=389,000 are used [59]. In both figures, the axial distance is non-dimensionalised by the tube length, *L*.

Consistent with wave cycle principles in shock tubes, the pressure plot shows a left-running expansion fan propagates to the driver section. Conversely, the solution shows an incident shock wave propagates to the right and eventually is reflected by the right wall. The reflected shock wave raises both pressure and temperature significantly and sufficiently high for thermal pyrolysis to be initiated in the driven section. The decomposition takes place slightly offset from the right wall, where the hot driver gas is in direct contact and mixed with the reactant gas. The $H_2$ distribution plot shows formation of hydrogen far away from the right wall and near to the contact surface between the compressed $CH_4$ and the $N_2$.
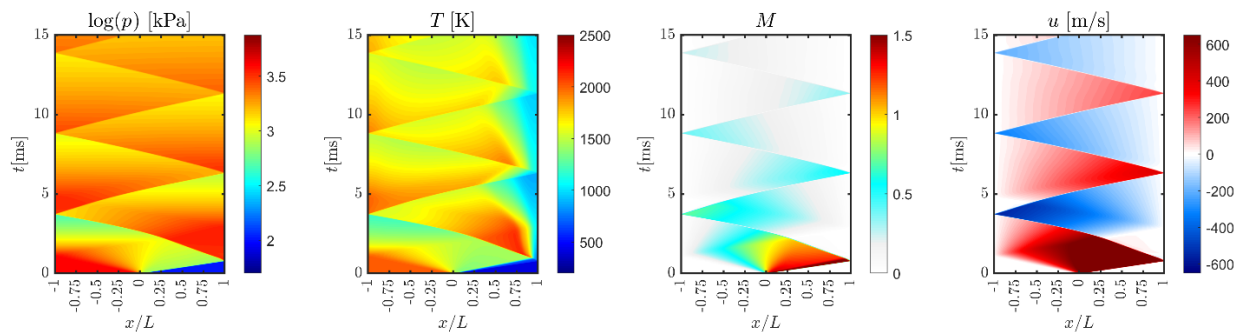


**Figure 19:** Contours of pressure plotted in logarithmic scale, temperature, Mach number and velocity in a shock tube as functions of time.

14
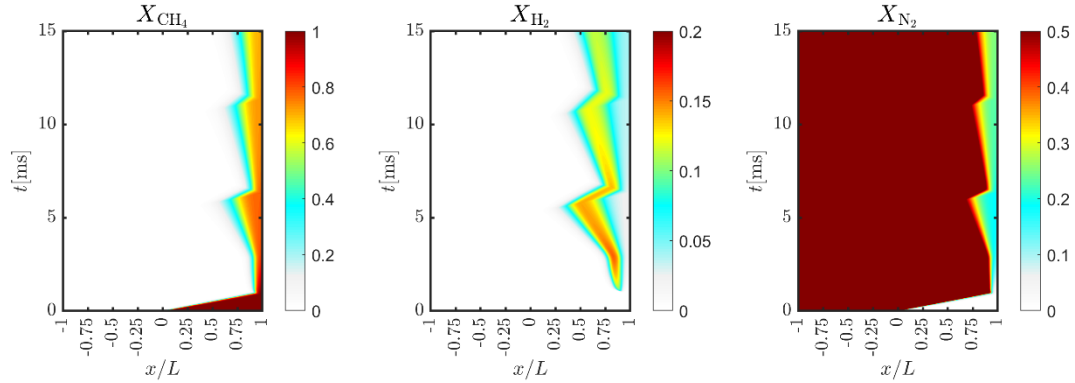
**Figure 20:** Mole fraction contours of methane (left), hydrogen (middle), and nitrogen (right) in a shock tube as functions of time.

Executing an equivalent shock-tube simulation with the lowest reaction rate in Fig. 18 given by Shantarovich et al. [60] ($A = 4.0\text{E}+11$ and $E_a=379,800$) and comparing the temperature and hydrogen mole fraction plots results in the delta plots shown in Fig. 21. Although exhibiting similar activation energies, the pre-exponential factor for the data of Kevorkian et al. [59] is approximately three orders of magnitude higher. These differences account for a 15% higher hydrogen mole fraction, as shown in Fig. 21 (left). Conversely, the increased reaction rate is accompanied by a stronger endothermic effect, where temperatures within the reacting stream differ by up to approximately 250 K, as indicated in Fig. 21 (right).
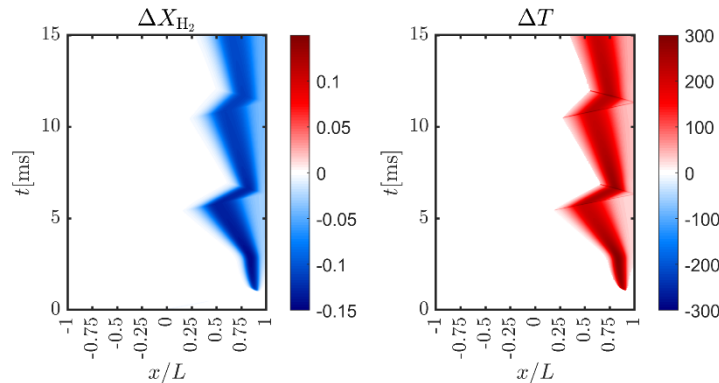


**Figure 21:** Delta plots for hydrogen (left) and temperature (right) between different kinetic reaction parameters for a shock tube solution.

After investigating the influence of the choice of kinetic parameters, modelling the wave dynamics within the wave reformer can be conducted more accurately. Since there are significant differences between the reaction rates reported in the literature, in this study a reaction rate was selected that lies in between the two extreme cases shown in the past shock tube studies, namely the coefficients introduced by Ref. [62], where $A = 1.3\text{E}+14$ and $E_a=422,900$ are proposed.

Figure 22 shows the resulting wave patterns of a four-port wave reformer with the port numbers correspond to those used in Fig. 17. In this example, the driver gas (hot, high-pressure nitrogen exiting the combustor at State 2) was chosen to enter the channel at 40 atm and 1700 K, and the driven gas (preheated methane) enters the channel at 6 atm and 773 K. The outlet pressure at port 3 is fixed at ambient pressure, while the flow conditions at port 7 are varied iteratively to ensure equal total pressure between ports 2 and 7, neglecting an unavoidable pressure loss across the combustor.

The contour plots indicate pressure value shown in logarithmic scale, temperature, Mach number and velocity as functions of time or azimuthal position (vertical axis) and position (horizontal) over one complete cycle of operation. The horizontal axis of each contour is again non-dimensional by the channel length (x/L). Vertical axis represented by angular displacement, $\theta$, is also non-dimensionalized by maximum angular displacement, $\theta_{max}$, which is 360 degrees. A color scale bar is provided to the immediate right of each contour plot. Similar to the shock tube simulations, the

15

wave pattern contours are accompanied by the species contours in Fig. 23. These mole fraction plots outline the spatial-temporal distribution of reactants ($CH_4$) and products ($H_2$) as well as the driver gas ($N_2$). In this simulation, the $CH_4$ plot shows the driven gas reaches approximately $x/L$=0.5 into the channel through opening of the inlet port 6 at non-dimensional time 0.8. Thus, when the cycle starts at non-dimensional time $\theta/\theta_{max} = 0$, about half of the channel is filled with the fresh driven gas ($CH_4$) and the remaining is filled with the residual driver gas ($N_2$) from a previous cycle.
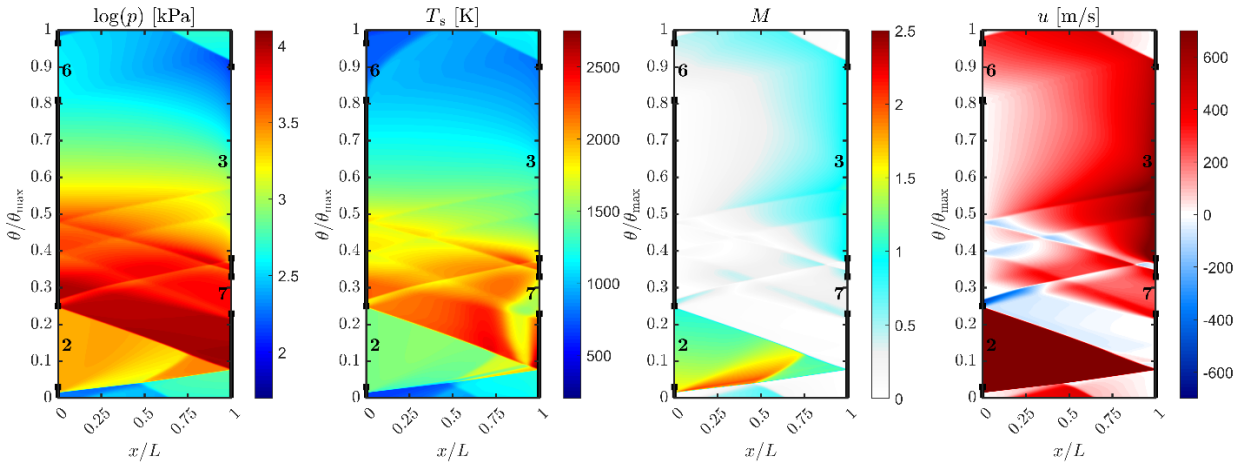


**Figure 22:** Contours of pressure plotted in logarithmic scale, temperature, Mach number and velocity in a four-port through-flow wave reformer.
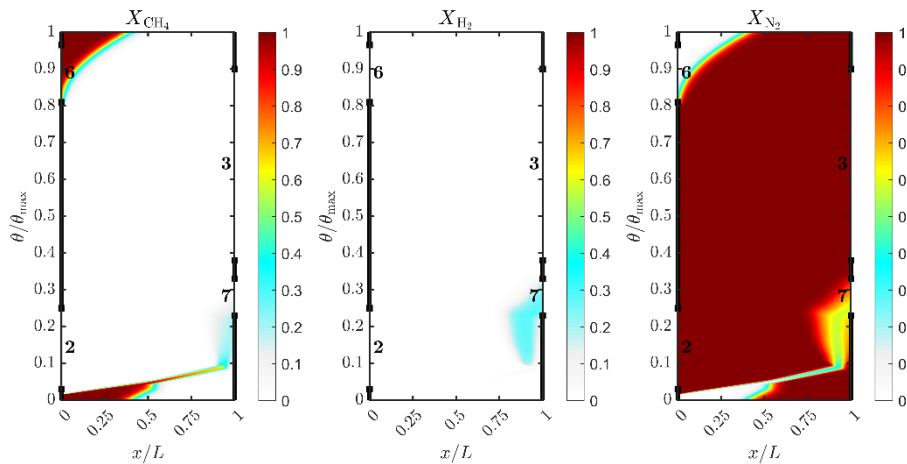


**Figure 23:** Species contour plots showing mole fraction of methane ($CH_4$), hydrogen ($H_2$), and nitrogen ($N_2$).

The pressure plot in Fig. 22 shows a strong incident shock wave is generated by exposing the channel to the high-pressure post-combustor flow at port 2. As the incident shock wave travels to the right of the channel, it collides with another left-running shock wave (i.e., hammer shock) that is generated upon closure of port 3 to the channel at non-dimensional time 0.9. The two shock waves meet at around $x/L = 0.5$ and in their wake both gas temperature and pressure experience a further increase prior to the arrival of the incident shock wave to the right endplate. A more significant higher-pressure region is also seen (dark red color) in a region behind a reflected shock wave created at non-dimensional time 0.1. On the pressure plot, the incidence, reflected, and the weak shock wave trajectories are clearly seen. A reduction in the channel pressure is also seen after opening port 3 at non-dimensional time about 0.4. A sufficiently long port width ensures the pressure within the channel can decrease in time for the low-pressure inlet at port 6 to inject the driven gas into the channel.
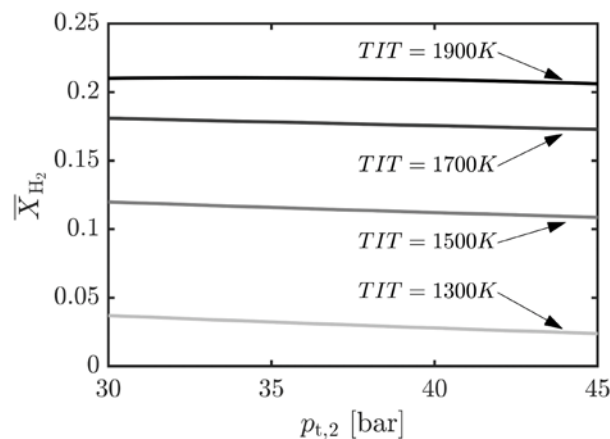
16

On the temperature plot, regions of high temperatures are seen behind the reflected shock wave. The impact of the temperature drop due to the endothermic effect is also seen between non-dimensional times 0.1-0.25 where the majority of pyrolysis happens. Further temperature reduction immediately after opening the product exhaust port 7 is associated with an expansion wave generated from the lower corner of port 7 propagating to the left, as described in Fig. 16.

The Mach number contour shows choked condition for the entire portion of the driver inlet port. The region with the highest Mach number (red color) is just behind the incidence shock wave before it collides with the hammer shock. The velocity plot shows how the reactant gas is stopped by the hammer shock when the driver outlet port closes at non-dimensional time 0.9 where the gas velocity goes to zero after it encounters the endplate (white color). Similarly, the velocity of the incoming driver gas also goes to zero near the right endplate by the reflected shock wave at non-dimensional time 0.1. Regions of zero velocities are seen near the left endplate located between non-dimensional times 0.25-0.80.

The reactant and hydrogen contour plots in Fig. 23 show that the driver gas pushes the driven gas towards the right side, where it mixes with the residual driver gas within the channel from the previous cycle. Thermal decomposition is initiated prior to the reflected shock wave just downstream of the aforementioned colliding shock wave system. However, the majority of pyrolysis takes place after the incident shock wave is reflected from the endplate, where hydrogen mole fraction reaches approximately 30% (light turquoise). Upon exhaust opening of the product, the produced hydrogen is purged. After opening and closing the outlet port 3 at non-dimensional times 0.4 and 0.9, respectively, the entire driver gas is still not completely purged, and some amount of nitrogen remains in the channel and is carried over to the next cycle.

Varying the total inlet pressure for different turbine inlet temperatures (TIT) and plotting this against the average hydrogen mole fraction through port 7 yields the curves given in Fig. 24. Obviously, TIT represents the driver gas temperature at port 2. Interestingly, the data shows relatively little sensitivity to the inlet pressure at port 2. In fact, the gradient at lower temperatures, such as 1300 and 1500 K, is slightly negative. This appears to weaken with increasing TIT, however. The reason for the negative gradient lies in the fact that by lowering the total inlet pressure at port 2, a better gas expansion capability of the low-pressure port 3 is achieved. Conversely, by increasing the driver gas inlet pressure, the port width at 3 is not large enough to expand the channel gas completely down to ambient conditions and some residual pressure remains within the channel before the driven gas intake port 6 opens. For a fixed driven gas inlet mass flow rate, this leads to a higher driven gas inlet pressure, which



**Figure 24:** Hydrogen mole fraction in port 7 outlet stream as function of driver gas inlet pressure and TIT.

eventually lowers the pressure ratio across incident and reflected shock waves. As a result, it can be concluded that at relatively elevated pressures in the range of 30 to 40 bar, a more effective shock heating-effect can be achieved through raising the driver temperature compared to the driver pressure.

## B. Producing fuel in-line for delivery to a gas turbine cycle:

Figure 25 shows a second exemplary turbine engine system where the wave reformer acts as a hydrogen-containing fuel production unit only. The wave reformer is supplied at the inlet port with pressurized, pre-heated fuel from a fuel source. In contrast to the first system, the feedstock could be a pipeline-pressure fluid (e.g., 40-100 atm), such as natural gas, rather than a burned gas. The combustor continues to receive high-pressure fuel product from the wave reformer and high-pressure air is still received from the compressor at its inlet. The turbine also still discharges a low-pressure exhaust gas that can provide heat to the heat exchanger. In this simpler arrangement, the conventional fossil fuel used in gas turbine engines is replaced by the hydrogen-containing fuel produced in the wave reformer. The new arrangement allows for a cleaner burning system with lower greenhouse gas emissions.
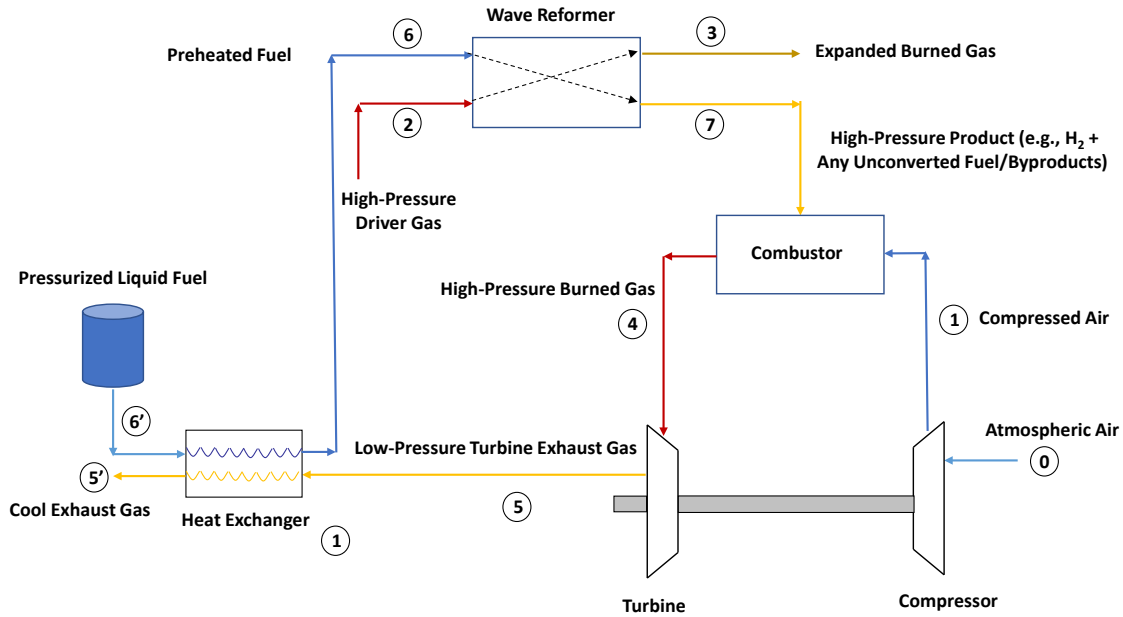
**Figure 25:** Wave reformer used for producing fuel in-line for delivery to a gas turbine cycle.

## C. Dual rotors integrated in a gas turbine cycle, producing fuel and pressure gain between compressor and turbine:

Figure 26 shows a third exemplary turbine engine cycle using a wave reformer, and a non-reacting four-port wave rotor placed between the compressor and turbine parallel to the burner. This system is similar to the system of Fig. 17, with the same descriptions, except that here a wave reformer and a separate wave rotor are used. Thus, Fig. 26 can be seen as a combination of Figs. 14 and 17. The wave rotor receives a large segment of the high-pressure burned gas from the combustor at its driver gas inlet port (State 3). The driven gas inlet port receives compressed air from the compressor (State 1). The doubly compressed air by the wave rotors is discharged back to the combustor (State 2). The burned gas, which has been expanded in the wave rotor, is discharged to the turbine (State 4). Here, in addition to a pressure gain produced between the compressed exit and turbine inlet by the wave rotor, the wave reformer provides hydrogen-containing product as fuel for the system. In this arrangement, the burned gas supplied to the turbine by the wave rotor is delivered at a higher pressure than in other power generation system arrangements. Consequently, more work can be extracted from the turbine with the wave rotor, leading to higher engine performance and a more efficient, cleaner burning power generation system. It is acknowledged that even though this method of use provides a high thermal efficiency and specific work and a low value of specific fuel consumption, concerns may be raised relative to the combustor design due to the elevation of the combustor pressure and temperature caused by the wave rotor addition. Operating a combustor under a higher pressure and temperature adds challenges in the aerodynamic and mechanical designs of current standard combustors. To address these difficulties, other topping cycles might be preferred as discussed in Ref. [64].

18
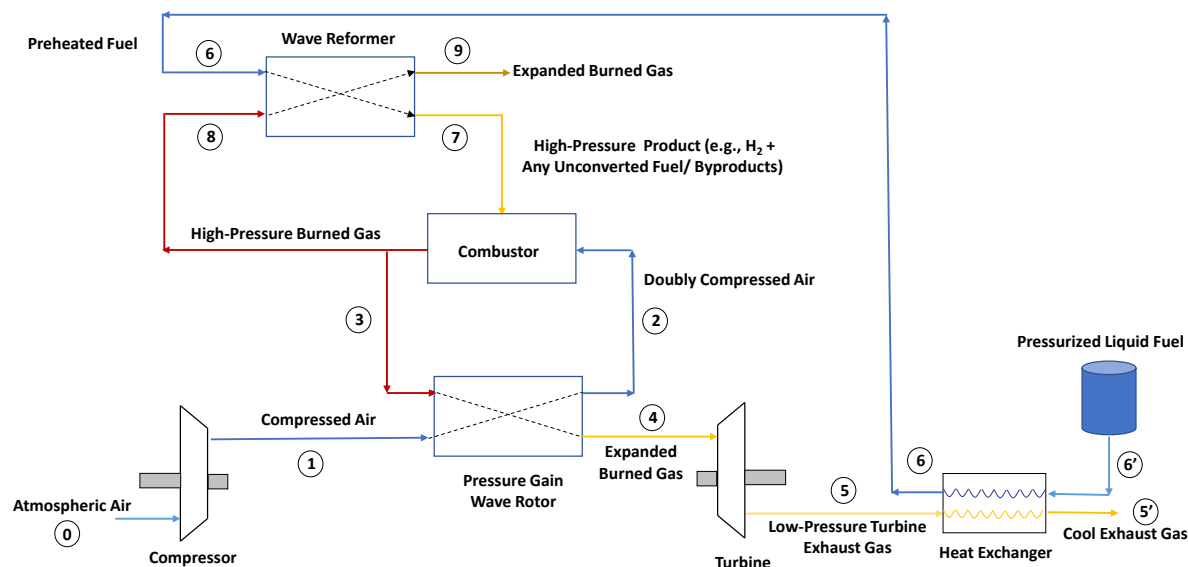
**Figure 26:** Dual rotors integrated in a gas turbine cycle, producing cleaner fuel and pressure gain between compressor and turbine.

## VI.    Conclusion

This paper introduced and discussed a novel power generation system combining a wave reformer, introduced by New Wave Hydrogen, Inc. (NWH$_2$), and a gas turbine in a flexible range of designs. The wave reformer is designed for continuously processing hydrocarbon fuel by the successive action of compression and expansion waves to produce hydrogen. The wave reformer consists of a drum that rotates past stationary inlet and outlet ports located at stationary walls on opposite ends of the reactor. The NWH$_2$ shock wave reformer completely departs from conventional pyrolysis technology because the reaction is induced by shock waves rather than electricity or other energy inputs. Using existing natural gas pipeline infrastructure, producing no direct CO$_2$ emissions, and with low electricity demand, the wave reformer holds promise for enabling a rapid transition to clean hydrogen production, with the potential for significant reductions in global greenhouse gas emissions. The purpose of this paper was to explore an application for this novel technology in gas turbine engines. The preliminary investigations supported by numerical modeling in a shock tube and in a shock wave reformer imply that integrating the NWH$_2$ wave reformer with a gas turbine could be an alternative solution for low-emission hydrogen-fueled gas turbine combustors.

## Acknowledgments

## References

[1] Fang, Z., Smith, R. L., and Qi, X., "Production of Hydrogen from Renewable Resources," in Biofuels and Biorefineries, Springer, 2015.

[2] Mondal, K. C., and Chandran, S. R., "Evaluation of the Economic Impact of Hydrogen Production by Methane Decomposition with Steam Reforming of Methane Process," *International Journal of Hydrogen Energy*, Vol. 39, No. 18, 2014, pp. 9670–9674.

[3] Muradov, N., "Low to Near-Zero CO$_2$ Production of Hydrogen from Fossil Fuels: Status and Perspectives," *International Journal of Hydrogen Energy*, Vol. 42, No. 20, 2017, pp. 14058–14088.

[4] Akbari, P., Copeland, C. D., Tüchler, S., Davidson, M., and Mahmoodi-Jezeh, S. V, "Shock Wave Heating: A Novel Method for Low-Cost Hydrogen Production" ASME Paper IMECE2021-69775, 2021.

[5] Akbari, P., Nalim, M. R., and Müller, N., "A Review of Wave Rotor Technology and Its Applications," *ASME Journal of Engineering for Gas Turbines and Power*, Vol. 128, No. 4, 2006, pp. 717-735.

[6] Azoury P. H., *Engineering Applications of Unsteady Fluid Flow*, John Wiley and Sons, New York, 1992.

[7] Rose, P. H., "Potential Applications of Wave Machinery to Energy and Chemical Processes," *Proceedings of the 12th International Symposium on Shock Tubes and Waves*, 1979, pp. 3-30.

[8] Shreeve, R. P., and Mathur, A., *Proceeding of the 1985 ONR/NAVAIR Wave Rotor Research and Technology Workshop*, Report NPS-67-85-008, Naval Postgraduate School, Monterey, CA, 1985.

[9] Kentfield, J. A. C., "Wave Rotors and Highlights of Their Development," AIAA Paper 98-3248, 1998.

[10] Welch, G. E., "Overview of Wave-Rotor Technology for Gas Turbine Engine Topping Cycles," *Novel Aero Propulsion Systems International Symposium, The Institution of Mechanical Engineers*, 2000, pp. 2-17.

[11] Pearson, R. D., "Pressure Exchangers and Pressure Exchange Engines," Chapter 16, *The Thermodynamics and Gas Dynamics of Internal Combustion Engines*, Vol. 1, Benson, R., Oxford University Press, 1982, pp. 903-940.

[12] Weber, H. E., *Shock Wave Engine Design*, John Wiley and Sons, New York, 1995.

[13] Weatherston, R. C., and Hertzberg, A., "The Energy Exchanger, A New Concept for High- Efficiency Gas Turbine Cycles," *Journal of Engineering for Power*, Vol. 89, No. 2, 1967, pp. 217-228.

[14] Taussig, R. T., and Hertzberg, A., "Wave Rotors for Turbomachinery," Winter Annual Meeting of the ASME, edited by Sladky, J. F., *Machinery for Direct Fluid-Fluid Energy Exchange*, AD-07, 1984, pp. 1-7.

[15] Zehnder, G., and Mayer, A., "Comprex® Pressure-Wave Supercharging for Automotive Diesels - State-of-the-Art," SAE Paper 840132, 1984.

[16] Hu, D., Yu, Y., Liu, P., Wu, X., and Zhao, Y., "Improving Refrigeration Performance by Using Pressure Exchange Characteristic of Wave Rotor," *ASME. Journal of Energy Resources Technology*, 141, No. 2, 2019, pp. 022004.

[17] Tüchler, S., and Copeland, C. D., "Validation of a Numerical Quasi-One-Dimensional Model for Wave Rotor Turbines with Curved Channels," *ASME Journal of Engineering for Gas Turbines and Power*, Vol. 142, No. 2, 2020, pp. 021017.

[18] Zehnder, G., Mayer, A. and Mathews, L., "The Free Running Comprex®," SAE Paper 890452, 1989.

[19] Seippel, C., "Pressure Exchanger," US Patent 2399394, 1946.

[20] Seippel, C., "Gas Turbine Installation," US Patent 2461186, 1949.

[21] Hussmann, A. W., "Pressure Exchanger with Combined Static and Dynamic Pressure Exchange," US Patent 2738123, 1956.

[22] Anonymous, "Pressure Exchanger Progress," *The Oil Engine and Gas Turbine*, Vol. 32, No. 371, 1964, pp. 35.

[23] Berchtold, M., and Gardiner, F. J., "The Comprex: A New Concept of Diesel Supercharging," ASME Paper 58-GTP-16, 1958.

[24] Pearson, R. D., "A Gas Wave-Turbine Engine Which Developed 35 HP and Performed Over a 6:1 Speed Range," *Proceeding of the 1985 ONR/NAVAIR Wave Rotor Research and Technology Workshop*, Report NPS-67-85-008, pp. 403-49, Naval Postgraduate School, Monterey, CA, 1985.

[25] Mathur, A., "A Brief Review of the GE Wave Engine Program (1958-1963)," *Proceeding of the 1985 ONR/NAVAIR Wave Rotor Research and Technology Workshop*, Report NPS-67-85-008, pp. 171-193, Naval Postgraduate School, Monterey, CA.,1985.

[26] Weber, H. E., "Wave Engine Aerothermodynamic Design," *ASME Journal of Engineering for Gas Turbines and Power*, Vol. 114, No. 4, 1992, pp. 790–796.

[27] Coleman, R. R., "Cycle for a Three-Stage Ultrahigh Pressure Ratio Wave Turbine Engine," AIAA Paper 94-2725, 1994,

[28] Tüchler, S., and Copeland, C. D., "Experimental and Numerical Assessment of an Optimized, Non-Axial Wave Rotor Turbine," *Applied Energy*, Vol. 268, 2020, pp. 115013.

[29] Welch, G. E., "Wave Engine Topping Cycle Assessment," AIAA Paper 97-0707, 1997.

[30] Welch, G. E., and Paxson, D. E., "Wave Turbine Analysis Tool Development," AIAA Paper 98-3402, 1998.

[31] Jagannath, R. R., Bane, S. P. M., and Razi Nalim, M., "Numerical Modeling of a Wave Turbine and Estimation of Shaft Work," *ASME Journal of Engineering for Gas Turbines and Power*, Vol. 140, No. 10, 2018, pp. 101106.

[32] Berchtold, M., and Lutz, T. W., "A New Small Power Output Gas Turbine Concept," ASME Paper 74-GT-111, 1974.

[33] Keller, J., "Gas Turbine Arrangement," US Patent 5220781, 1993.

[34] Zauner, E., Chyou, Y. P., Walraven, F., and Althaus, R., "Gas Turbine Topping Stage Based on Energy Exchangers: Process and Performance," ASME Paper 93-GT-58,1993.

[35] Berchtold, M., "The Comprex®," *Proceeding of the 1985 ONR/NAVAIR Wave Rotor Research and Technology Workshop*, Report NPS-67-85-008, pp. 50-74, Naval Postgraduate School, Monterey, CA, 1985.

[36] Taussig, R. T., "Wave Rotor Turbofan Engines for Aircraft," Winter Annual Meeting of the ASME, edited by Sladky, J. F., *Machinery for Direct Fluid-Fluid Energy Exchange*, AD-07, 1984, pp. 9-45.

[37] Taussig, R., Cassady, P., Zumdieck, J., Thayer, W. and Klosterman, E., "Investigation of Wave Rotor Turbofans for Cruise Missile Engines," Final Report Submitted by MSNW to DARPA, Contract No. N00140-82-C-9729, 1983.

[38] Zumdiek, J. F., Thayer, W. J., Cassady, P. E., Taussig, R. T., Christiansen, W. H., and Hertzberg, A., "The Energy Exchanger in Advanced Power Cycle Systems," *Proceeding of the 14th Intersociety Energy Conversion Engineering Conference*, 1979.

[39] Zumdiek, J. F., Vaidyanathan, T. S., Klosterman, E. L., Taussig, R. T., Cassady, P. E., Thayer, W. J., and Christiansen, W. H., "The Fluid Dynamic Aspects of an Efficient Point Design Energy Exchanger," *Proceeding of the 12th International Symposium on Shock Tubes and Waves*, 1979.

[40] Thayer, W. J., and Taussig, R. T., "Erosion Resistance and Efficiency of Energy Exchangers," ASME Paper 82-GT-191, 1982.

[41] Hertzberg, A., "Nitrogen Fixation for Fertilizers by Gasdynamic Techniques," *Proceedings of the 10th International Shock Tube Symposium*, 1975, pp. 17-28.

[42] Christiansen, W. H., and Hertzberg, A., "Wave Machinery for Chemical Processing and High-Efficiency Heat Engines," *Proceedings of the 20th International Symposium on Shock Waves*, 1995, pp. 135-139.

[43] Wilson J., Fronek, D., "Initial Results from the NASA-Lewis Wave Rotor Experiment," AIAA Paper 93-2521, 1993.

[44] Kentfield, J. A. C., *Nonsteady, One-Dimensional, Internal, Compressible Flows*, Oxford University Press, Oxford, 1993.

[45] Resler, E. L, Moscari, J. C., and Nalim, M. R., "Analytic Design Methods for Wave Cycles," *AIAA Journal of Propulsion and Power*, Vol. 10, No. 5, 1994, pp. 683-689.

[46] Paxson, D. E., "Comparison Between Numerically Modeled and Experimentally Measured Wave-Rotor Loss Mechanism," *Journal of Propulsion and Power*, Vol. 11, No. 5, 1995, pp. 908-914.

[47] Welch, G. E., "Two-Dimensional Computational Model for Wave Rotor Flow Dynamics," *Journal Engineering for Gas Turbines and Power*, Vol. 119, No. 4, 1997, pp. 978-985.

[48] Paxson, D. E., Wilson, J., and Welch, G. E., "Comparison Between Simulated and Experimentally Measured Performance of a Four Port Wave Rotor," AIAA Paper 2007-5049, 2007.

[49] Wilson, J., Welch, G. E., and Paxson, D. E., "Experimental Results of Performance Tests on a Four-Port Wave Rotor," AIAA Paper 2007-1250, 2007.

[50] Welch, G. E., Jones, S. M. and Paxson, D. E., "Wave Rotor-Enhanced Gas Turbine Engines," *Journal of Engineering for Gas Turbines and Power*, Vol. 119, No. 2, 1997, pp. 469-477.

[51] Snyder, P. H., and Fish, R. E., "Assessment of a Wave Rotor Topped Demonstrator Gas Turbine Engine Concept," ASME Paper 96-GT-41, 1996.

[52] Campbell, M. F., Parise, T., Tulgestke, A. M. et al., "Strategies for Obtaining Long Constant-pressure Test Times in Shock Tubes," Shock Waves, Vol. 25, 2015, pp. 651–665.

[53] Tüchler, S., and Copeland, C. D., "Parametric Numerical Study on the Performance Characteristics of a Micro-Wave Rotor Gas Turbine," International Gas Turbine Congress, Paper IGTC-2019-200, 2019.

[54] Napier, D. H., and Subrahmanyam, N., "Pyrolysis of Methane in a Single Pulse Shock Tube," *Journal of Applied Chemistry and Biotechnology*, Vol. 22, 1972, pp. 303-317.

[55] Gardiner Jr., W. C., and Owen, J. H., "Rate and Mechanism of Methane Pyrolysis from 2000° to 2700° K," *Symposium (International) on Combustion*, Vol. 15, Issue 1, 1975, pp. 857-868.

[56] Kassel, L.S., "The Thermal Decomposition of Methane," *Journal of the American Chemical Society*, Vol. 54, 1932, pp. 3949-3962.

[57] Skinner, G. B., and Ruehrwein, R. A., "Shock Tube Studies on the Pyrolysis and Oxidation of Methane," *The Journal of Physical Chemistry*, Vol. 63, 1959, pp. 1736-1742.

[58] Glick, H. S., "Shock Tube Studies of Reaction Kinetics of Aliphatic Hydrocarbons*," 7th Symposium (International) on Combustion*, Vol. 7, No. 1, 1959, pp. 98-107

[59] Kevorkian, V., and Heath, C. E., "The Decomposition of Methane in Shock Waves," *The Journal of Physical Chemistry*, Vol. 64, Issue 8, 1960, 964-968.

[60] Shantarovich, P. S., and Pavlov, B. V., "Thermal Cracking of Methane," *International Chemical Engineering*, Vol. 2, Issue 3, 1962, pp. 415-418.

[61] Kozlov, G. I., and Knorre, V. G., "Single-Pulse Shock Tube Studies on the Kinetics of the Thermal Decomposition of Methane," *Combustion and Flame*, Vol. 6, 1962, pp. 253-263.

[62] Palmer, H. B., and Hirt, T.J., "The Activation Energy for the Pyrolysis of Methane," *The Journal of Physical Chemistry*, Vol. 67, 1963, pp. 709-711.

[63] Palmer, H. B., and Lahaye, J., "On the Kinetics and Mechanism of the Thermal Decomposition of Methane in a Flow System," *The Journal of Physical Chemistry*, Vol. 72, 1968, pp. 348-353.

[64] Akbari, P., Müller, N., and Nalim, M. R., "Performance Enhancement of Microturbine Engines Topped with Wave Rotors," *ASME Journal of Engineering for Gas Turbines and Power*, Vol. 128, No. 1, 2006, pp. 190-202.